RSC Advances

PAPER

Cite this: *RSC Adv.*, 2019, **9**, 11552

Carbon nitride supported $Ni_{0.5}Co_{0.5}O$ nanoparticles with strong interfacial interaction to enhance the hydrolysis of ammonia borane†

Yunpeng Shang,[a] Kun Feng,[a] Yu Wang,*[b] Xuhui Sun [a] and Jun Zhong *[a]

Received 7th March 2019
Accepted 3rd April 2019

DOI: 10.1039/c9ra01743g

rsc.li/rsc-advances

Ammonia borane (AB) is an ideal hydrogen-storage material for fuel cells but its application has been strongly limited by using rare noble-metal-based catalysts. Here we have prepared a hybrid material of $Ni_{0.5}Co_{0.5}O$ nanoparticles on nitric-acid treated carbon nitride (NCN) for the hydrolysis of AB. The $Ni_{0.5}Co_{0.5}O$-NCN catalyst achieves a high total turnover frequency (TOF) value of 76.1 (H_2) mol per (Cat-metal) mol min in pure water at room temperature, with a good stability by keeping 83.2% activity after 6 runs. The TOF is comparable to the best values ever reported for noble-metal-free catalysts without extra conditions such as light illumination or a strong alkaline environment. Synchrotron radiation based X-ray absorption spectroscopy reveals that the carbon nitride substrate has two reaction centers to form stable interfacial interaction with the NPs, in which carbon can act as the electron acceptor while nitrogen acts as the electron donor. Thus the NP-NCN system has a hybridized electronic structure which is favorable for the catalytic reaction to produce hydrogen. In-depth understanding of the interfacial interaction between NCN and NPs may also shed light on the mechanism study of various energy-related applications based on carbon nitride.

Introduction

Hydrogen has been used as a clean and sustainable energy source for fuel cells.[1–3] However, its storage and release under mild conditions are still big problems.[3–9] Ammonia borane (AB) is considered as an excellent hydrogen-storage material with a high hydrogen content (19.6 wt%). Moreover, AB is nontoxic and stable in aqueous solutions at room temperature.[3–13] The release of hydrogen from AB under mild conditions has been widely studied, which is convenient and very efficient when using catalysts based on noble metal elements (such as Ag, Pt, or Ru). However, the consumption of expensive and rare noble metals strongly limits the practical applications.[6–14] The investigation of non-noble metal-based catalysts for the hydrolysis of AB is thus highly required.[6–14]

Various methods were reported to prepare efficient catalysts with low cost.[7–16] For example, Ni nanoparticles (NPs) with more active sites were synthesized by removing the surfactant, and showed a total turnover frequency (TOF) value of 30.7 (H_2) mol per (Cat-Ni) mol min.[7] The combination of non-noble metal and phosphorus was also reported as an excellent catalyst for the hydrolysis of AB.[8,15,16] In particular, Chen *et al.* recently reported a very efficient Ni–Co–P catalyst on graphene oxide (GO) to achieve a high TOF value of 109.4 (H_2) mol per (Cat-metal) mol min.[15] The high TOF value also benefited from the strong alkaline environment.[15–18] Except for the optimized catalyst content and special reaction environments, the selection of a good substrate for the catalysts was also very important for the performance.[19–22] For example, recently we showed that GO was a good supporting material to anchor the NPs with strong interfacial interaction, which could lead to a high TOF value of 70.0 (H_2) mol per (Cat-metal) mol min for the hydrolysis of AB in water.[19]

Currently, carbon nitride (C_3N_4) is widely studied as an excellent supporting material for various energy related applications.[23–25] Carbon nitride was also used to support NPs for the hydrolysis of AB.[25–28] For example, Au–Co NPs on carbon nitride were reported to remarkably enhance the catalytic hydrolysis of AB with a favorable Motty–Schottky effect at the metal–semiconductor interface.[26] Recently, Su *et al.* reported the deposition of CuCo NPs on C_3N_4 to get a TOF value of 40.5 (H_2) mol per (Cat-metal) mol min.[27] Moreover, the TOF value could be greatly enhanced to 75.1 (H_2) mol per (Cat-metal) mol min under visible light illumination due to the charge transfer from C_3N_4 to NPs. The charge transfer could be further enhanced by modifying C_3N_4 with enlarged surface area or extended light absorption.[28] Although carbon nitride was widely used for the

[a]*Institute of Functional Nano and Soft Materials Laboratory (FUNSOM), Jiangsu Key Laboratory for Carbon-Based Functional Materials and Devices, Soochow University, Suzhou 215123, China. E-mail: jzhong@suda.edu.cn*

[b]*Shanghai Synchrotron Radiation Facility, Shanghai Advanced Research Institute, Chinese Academy of Sciences, Shanghai 201204, China. E-mail: wangyu@sinap.ac.cn*

† Electronic supplementary information (ESI) available: Particle size distribution, XRD and FTIR spectra, dependence of the hydrolysis reaction on $Ni_{0.5}Co_{0.5}O$-NCN/AB molar ratios, XPS spectra, tables for the TOF values. See DOI: 10.1039/c9ra01743g

hydrolysis of AB,[25–28] it was mainly considered as a good light absorption material to enhance the electron density, while the substrate effect and the interfacial interaction between NPs and carbon nitride have been rarely studied.

Here we prepare a hybrid material of $Ni_{0.5}Co_{0.5}O$ NPs deposited on nitric-acid treated carbon nitride (NCN) for the hydrolysis of AB. Interestingly, the NCN substrate shows a strong interfacial interaction with the $Ni_{0.5}Co_{0.5}O$ NPs according to synchrotron radiation based X-ray absorption spectroscopy (XAS), in which the carbon atoms in NCN may act as the electron acceptor while the nitrogen atoms act as the electron donor to anchor the NPs. Thus the NP-NCN system has a hybridized electronic structure favorable for the catalytic reaction to release hydrogen. Actually, the $Ni_{0.5}Co_{0.5}O$-NCN catalyst achieves a high TOF value of 76.1 (H_2) mol per (Cat-metal) mol min in pure water at room temperature, with a good stability by keeping 83.2% activity after 6 runs. It should be noted that this value was obtained without any extra conditions such as light illumination or strong alkaline environment, indicating that the high efficiency of this catalyst might be used for the practical condition in fuel cells. Moreover, the strong interfacial interaction between NCN and NPs may also shed light on the mechanism study of various applications based on carbon nitride.

Experimental section

Materials preparation

Bulk carbon nitride was synthesized by calcining melamine (10 g) at 823 K (10 K min^{-1} ramp rate) for 4 h in a muffle furnace. Exfoliated carbon nitride was obtained *via* the thermal exfoliation of bulk carbon nitride (3 g) at 773 K (5 K min^{-1} ramp rate) for 2 h in air. Nitric-acid treated carbon nitride was prepared as reported in the literature.[29] In brief, 1 g bulk carbon nitride powder was put into the solution of 100 mL HNO_3 (5 mol L^{-1}) and refluxed for 24 h at 125 °C. After cooling to room temperature, the product was centrifuged and washed until pH = 7. The product was finally freeze-dried at −80 °C. To deposit $Ni_{0.5}Co_{0.5}O$ NPs on NCN, 0.01 mmol $NiCl_2 \cdot 6H_2O$ and 0.01 mmol $CoCl_2.6H_2O$ were mixed with 2.5 mg NCN powder and 2 mL deionized water in a flask. Then the solution was sonicated for 30 minutes. 0.5 mL solution with ammonia borane (0.5 mmol) and sodium borohydride (0.02 mmol) was then slowly added in the mixture. The obtained powder was washed and freeze-dried in air for 12 hours. Then the final product was labeled as $Ni_{0.5}Co_{0.5}O$-NCN (0.5 : 0.5 stands for the precursor ratio, which is similar to the ICP data; O means an oxidized state of the NPs due to the exposure to air, which has been revealed by XPS and XAS). Different metals (such as Cu, Ni, Co) with various precursor ratios (for example, $Ni_xCo_{1-x}O$-NCN) were also used to prepare the NPs on NCN for comparison.

Structural characterization

High-resolution transmission electron microscope (HRTEM) (FEI Tecnai G2 F20 S-TIWN), Fourier transform microscopy infrared spectrometer (FTIR, VERTX 70), X-ray diffraction (XRD, PANalytical B.V. Empyrean powder diffractometer equipped with PIXcel3D detector) and X-ray photoelectron spectrometer (XPS, Kratos AXIS UltraDLD) were used for the structure characterization. X-ray absorption spectroscopy (XAS) experiments were performed at the Shanghai Synchrotron Radiation Facility (SSRF, 14W and 08U), the National Synchrotron Radiation Laboratory (NSRL, XMCD and Photoemission beamlines) and the Taiwan Light Source (TLS, 01C and 17C). The metal contents were measured by an inductively coupled plasma optical emission spectrometer (ICP-OES, VISTA-MPX (CCD Simultaneous ICPOES), Varian).

Catalytic activity measurement

A round-bottom flask with one sealed neck (25 mL) connected to a gas-collection tube was used for the hydrolysis reaction.[19,20] In a typical case, 5.0 mg catalyst powder with 2 mL deionized water was put into the flask and sonicated for 30 minutes. Then 0.5 mL AB (1 mmol mL^{-1}) water solution (for $Ni_{0.5}Co_{0.5}O$-NCN, $n_{metal} : n_{AB} = 0.04$ according to the ICP data) was quickly injected into the flask. The reaction temperature was controlled at room temperature. The reaction time was recorded when observing the first bubble in a few seconds. The hydrogen amount was measured by recording the displaced water. Typically, the hydrolysis reaction follows the formula: $NH_3BH_3 + 4H_2O = NH_4^+ + B(OH)_4^- + 3H_2$ and the TOF numbers can thus be calculated according to another formula: $TOF = n_{H_2}/(n_{metal} \times t)$. n_{H_2} is the mole number of H_2 and n_{metal} is the total mole number of metal (Ni and Co). t represents the completed reaction time (min).

Results and discussion

The catalytic property of $Ni_{0.5}Co_{0.5}O$-NCN for the hydrolysis of AB is shown in Fig. 1. The hydrogen evolution curves of $Ni_{0.5}Co_{0.5}O$-NCN with a comparison to that of single metal based materials CoO-NCN and NiO-NCN are shown in Fig. 1a while Fig. 1b shows a comparison of various $Ni_xCo_{1-x}O$-NCN samples with different Ni : Co precursor ratios. The hydrolysis process of $Ni_{0.5}Co_{0.5}O$-NCN can be quickly finished in about 1 minute (3 mole hydrogen produced from 1 mole AB, $n_{metal} : n_{AB} = 0.04$). The TOF values of various samples are calculated according to the measured ICP data and shown in Table S1.† Pure NCN shows no catalytic activity for the hydrolysis of AB (TOF = 0). When loading with different kinds of NPs, the NP-NCN hybrids exhibit different catalytic performance. For the samples with only Co or Ni metals (only Co or Ni precursor with the same preparation process), both CoO-NCN and NiO-NCN show a relatively low activity in Fig. 1a (TOF values are 5.5 and 13.3 (H_2) mol per (Cat-M) mol min in Table S1,† respectively). However, when two metal elements are used to form the bimetallic NPs, a synergistic effect can be observed and the catalytic activity can be greatly enhanced.[19] All the $Ni_xCo_{1-x}O$-NCN samples show a TOF value higher than 35 (H_2) mol per (Cat-M) mol min (also see Fig. 1b). Moreover, the $Ni_{0.5}Co_{0.5}O$-NCN with a balance Ni : Co ratio shows the best performance with an excellent TOF value of 76.1 (H_2) mol per (Cat-M)

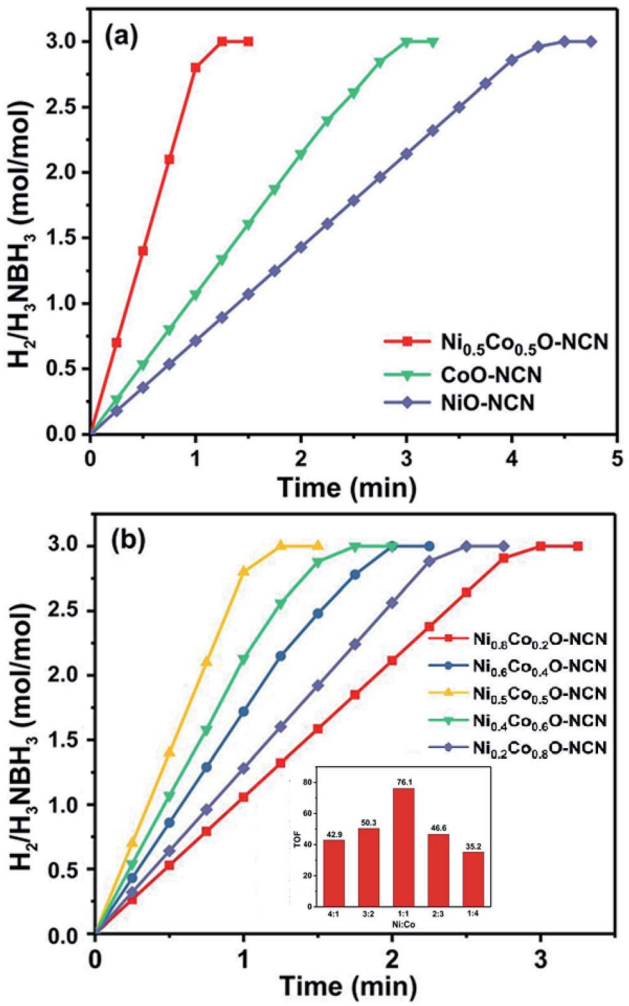

Fig. 1 (a) Hydrogen evolution curves of the hydrolysis of AB aqueous solution catalyzed by $Ni_{0.5}Co_{0.5}O$-NCN, CoO-NCN and NiO-NCN. (b) Hydrogen evolution curves catalyzed by the $Ni_xCo_{1-x}O$-NCN samples with different Ni : Co ratios (the first bubble can be observed in a few seconds). The inset also compares the TOF values.

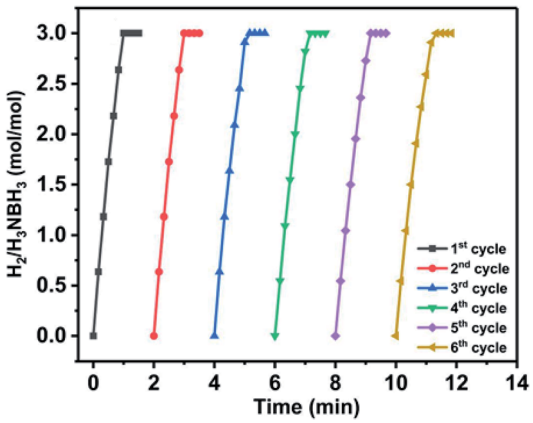

Fig. 2 Stability test of $Ni_{0.5}Co_{0.5}O$-NCN in 6 runs for the hydrolysis of AB. The TOF value decreases from 76.1 to 63.3 (the 6th cycle, 83.2% left).

mol min, which is also comparable to the best values ever reported in the literatures for noble-metal-free catalysts (without light and strong alkaline solution). A comparison of the TOF values with the literatures is also shown in the ESI Table S2.† As reported in the literatures,[19–22] the excellent catalytic performance of the hybrids could be attributed to the synergistic effect of the two metal elements and the interfacial interaction between NPs and the supporting material. However, only GO based supporting materials have been widely studied while the interfacial interaction between NPs and carbon nitride based materials has not been clearly understood yet.

The stability curves of $Ni_{0.5}Co_{0.5}O$-NCN are shown in Fig. 2. After 6 cycles, the TOF value can remain at a good value of 63.3 (H_2) mol per (Cat-M) mol min (83.2%, Fig. 2 and Table S3†), suggesting a good stability of $Ni_{0.5}Co_{0.5}O$-NCN. Various metal compositions such as Cu and Co or Cu and Ni are also used to get the optimized catalyst. The catalytic performances are shown in Fig. S1a† while the combination of Ni and Co in $Ni_{0.5}Co_{0.5}O$-NCN shows the best performance. Fig. S1b† also compares the catalytic performance by using different substrates such as CN and NCN and the sample with NCN substrate shows a much better performance.

The temperature dependence of the catalytic reaction is also shown in Fig. S2.† The catalytic performance sharply increases with the increased temperature, which is consistent with the literatures.[8,19] The inset shows the Arrhenius plot and the activation energy of $Ni_{0.5}Co_{0.5}O$-NCN can thus be calculated to be a low value 43.18 kJ mol^{-1}, which may also favorite the performance.[8] It should be noted that since the reaction can be quickly finished at a higher temperature, in this test we only use 2.5 mg catalyst powder for the hydrolysis. Fig. S3a and S3b† show the hydrolysis reaction evolution on $Ni_{0.5}Co_{0.5}O$-NCN/AB molar ratios when keeping the AB amount constant at 298 K, while in Fig. S3c and S3d† the amount of $Ni_{0.5}Co_{0.5}O$-NCN keeps a constant value to probe the relationship between hydrogen-generating rate and AB concentration. In Fig. S3b† the logarithmic plot of the calculated initial reaction rate *versus* the concentration of the catalyst shows a positive slope of 0.994, suggesting a first-order kinetics similar to the literatures.[8,19] Interestingly, the hydrolysis reaction with respect to AB concentration does not follow the zero-order kinetics (a positive slope of 0.064), which might be attributed to the interaction between water and the catalyst.[8,19]

The structure characterization of $Ni_{0.5}Co_{0.5}O$-NCN has been shown in Fig. 3 with the HRTEM image and elemental mappings. Nitric-acid treated carbon nitride has been used as the supporting material and the deposition of Ni and Co based NPs on NCN can be clearly observed in Fig. 3a. The average particle size in Fig. 3a is 2.8 nm and the particle size distribution is also shown in the ESI Fig. S4.† Dark field TEM image and the corresponding elemental mappings are shown in Fig. 3, which strongly confirm the uniform distribution of both Ni and Co in the NPs. The similar elemental mappings of Ni and Co suggest that Ni and Co may form a bimetallic alloy structure in the NPs. However, it could be an oxidized alloy structure as discussed with further characterizations such as XPS and XAS.

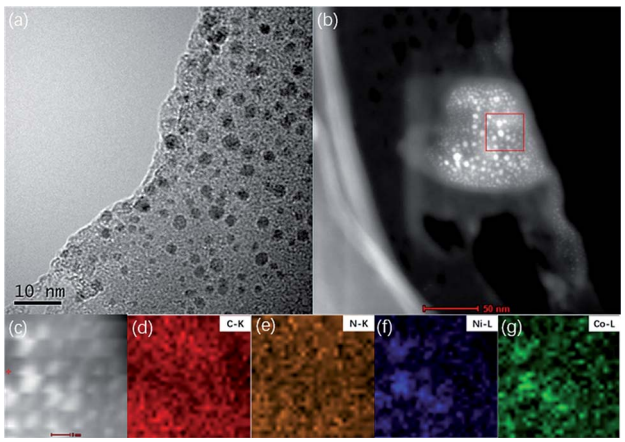

Fig. 3 (a) HRTEM image of $Ni_{0.5}Co_{0.5}O$-NCN. (b), (c) and (d–g) Dark field TEM images and the corresponding elemental mappings of $Ni_{0.5}Co_{0.5}O$-NCN: C (red), N (yellow), Ni (blue) and Co (green).

The carbon nitride structure as supporting material in $Ni_{0.5}Co_{0.5}O$-NCN is also confirmed by the XRD spectra in Fig. S5.† The original CN shows a feature at around 13.2° corresponding to the (100) plane.[30] A sharp feature at around 26.4° can also be observed for the (002) plane, which can be attributed to the stacking of the conjugated aromatic system.[30–32] The XRD spectrum of CN is very similar to the data in literatures, confirming the carbon nitride structure. NCN and $Ni_{0.5}Co_{0.5}O$-NCN show similar XRD spectra as that of CN. Slight shifts of the (002) peak for NCN and $Ni_{0.5}Co_{0.5}O$-NCN can also be observed, which can be attributed to the nitric acid treatment leading to a dense packing.[32] No additional XRD peaks for Ni or Co based materials in $Ni_{0.5}Co_{0.5}O$-NCN can be observed, which can be attributed to the small particle size of NPs on NCN. FTIR spectra of CN and NCN are also shown in Fig. S6† to confirm the carbon nitride structure. The broad band at 3165 cm^{-1} can be attributed to the intermolecular hydrogen bonding of the primary and secondary amines and the O–H bonds of water.[33] The features located in the range of 1239–1647 cm^{-1} can be assigned to the C–N stretching of g-C_3N_4 and the feature at 810 cm^{-1} can be related to tri-*s*-triazine.[34] The FTIR spectrum of $Ni_{0.5}Co_{0.5}O$-NCN also shows similar features as that for CN and NCN (data not shown). Both XRD and FTIR confirm that the supporting material used here has the carbon nitride structure.

XPS and synchrotron radiation based XAS are used to probe the electronic structure of $Ni_{0.5}Co_{0.5}O$-NCN. From the TEM image it is clear that Ni and Co are uniformly distributed in the NPs suggesting a bimetallic structure. However, it is still not clear about the chemical states. Here in Fig. S7c and S7d† the XPS spectra of $Ni_{0.5}Co_{0.5}O$-NCN at Ni and Co 2p edges are shown, respectively. Interestingly, both Ni and Co show oxidized chemical states similar to that of NiO and CoO, suggesting the formation of an oxidized hybrid structure. The XAS spectra at Ni and Co L-edges in the ESI Fig. S8† also confirm the oxidized chemical states of Ni and Co in $Ni_{0.5}Co_{0.5}O$-NCN. According to the similar contents of Ni and Co in the NPs (from ICP and the similar distribution), we thus assign the NPs as $Ni_{0.5}Co_{0.5}O$. The electronic structure of supporting material is also revealed in Fig. S7a and S7b† at the C and N 1s edges, respectively. In Fig. S7a† the sharp peak at 287.8 eV can be attributed to the graphitic carbon in carbon nitride with typical C–N–C bonds.[35–37] The weak feature at 284.6 eV can be attributed to the possible defect sites with sp^2 carbon structure. The two features located at around 398.2 eV and 400.5 eV in Fig. S7b† can be assigned to the pyridinic type and graphitic type N species in the C_3N_4 ring structure, respectively.[35,36] The XPS spectra is consistent with the XRD and FTIR results confirming the carbon nitride structure in the $Ni_{0.5}Co_{0.5}O$-NCN sample.

More information can be obtained from the XAS spectra at C and N K-edges in Fig. 4. Fig. 4a shows the C K-edge XAS spectra of pure NCN and $Ni_{0.5}Co_{0.5}O$-NCN. There are mainly three features labeled as A (A1 and A2), B and D for pure NCN. According to the literatures,[36–39] the main features B (around 288.2 eV) and D (around 294 eV) can be attributed to the π* and σ* excitations of C–N–C bonds in the C_3N_4 structure, respectively. The C K-edge XAS spectrum suggests that NCN has a good carbon nitride structure. The features A1 and A2 at around 285.4 eV are very weak, which can be attributed to the π* excitation of C=C bonds at the defect sites.[36–39] $Ni_{0.5}Co_{0.5}O$-NCN

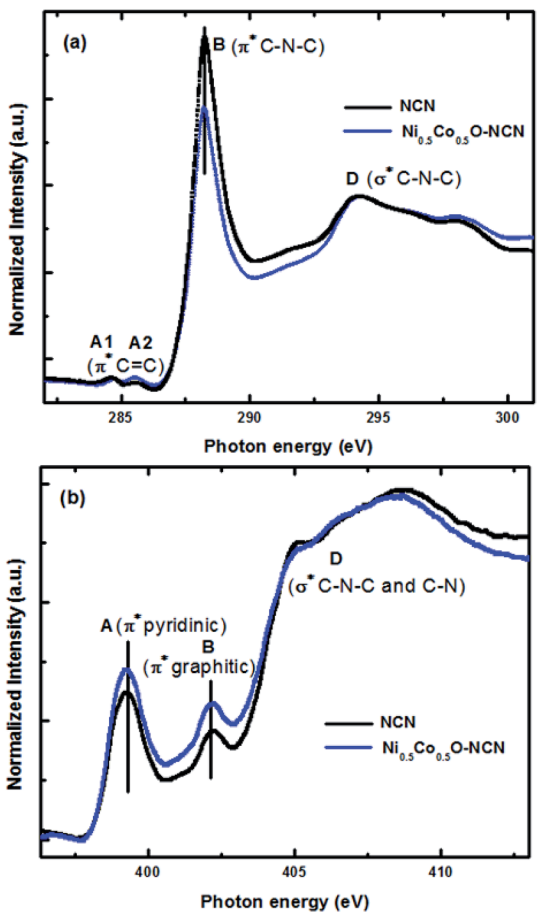

Fig. 4 XAS spectra of $Ni_{0.5}Co_{0.5}O$-NCN and the reference samples at C K-edge (a) and N K-edge (b), respectively.

shows similar XAS features suggesting a similar substrate structure as that of NCN. However, a decreased intensity of feature B for $Ni_{0.5}Co_{0.5}O$-NCN can be observed when compared to that of NCN, suggesting the interfacial interaction between $Ni_{0.5}Co_{0.5}O$ NPs and NCN. Typically, the XAS feature stands for the intensity of unoccupied state in the material and the decrease of feature B suggests the filling of electrons to the unoccupied state of carbon.[37,39] It means that carbon in NCN may get some electrons from the $Ni_{0.5}Co_{0.5}O$ NPs with the formation of interfacial interaction between NPs and NCN.

Interestingly, from the N K-edge XAS spectra in Fig. 4b we can also find the similar interfacial effect. According to the literatures,[36–39] features A and B at N K-edge can be assigned to the π^* excitations of pyridinic type and graphitic type N species in the C_3N_4 ring structure, respectively. A broad feature D can also be observed, which can be attributed to the σ^* excitation of C–N–C or C–N (N–3C bridgings) bonds.[36–39] It is clear that $Ni_{0.5}Co_{0.5}O$-NCN shows increased intensity of features A and B when compared to that of NCN, suggesting increased unoccupied states at the N sites. N may lose electrons with the interfacial interaction. The XAS results at both N and C K-edges reveal that in $Ni_{0.5}Co_{0.5}O$-NCN the N sites may act as the electron donor to the NPs while the C sites can act as the electron acceptor from the NPs. Thus a stable interfacial interaction with the hybridized electronic structure can be constructed between NPs and NCN, which may significantly favorite the catalytic reaction.[19] It could also be the reason for carbon nitride to act as a good supporting material in various applications. The two elements of C and N in carbon nitride can thus act as two different bonding sites to anchor the NPs with enhanced performance.

Fig. S8† also shows the XAS spectra of $Ni_{0.5}Co_{0.5}O$-NCN at Ni and Co L-edges with a comparison to the reference samples. However, since the particle size in $Ni_{0.5}Co_{0.5}O$-NCN is obviously smaller than that in the bulk reference samples (NiO or CoO), we cannot clearly identify the interfacial interaction from the size effect in the metal L-edge XAS spectra. We also show the XAS spectra of $Ni_{0.5}Co_{0.5}O$-NCN at Ni and Co K-edges with a comparison to the reference samples in Fig. S9.† The chemical states of Ni and Co in $Ni_{0.5}Co_{0.5}O$-NCN before the hydrolysis reaction are very similar to that of NiO and CoO, confirming our results. It should be noted that it is still hard to observe the interfacial interaction from the hard X-ray XAS spectra. Thus the soft X-ray XAS study at both C and N K-edges seems to be a very suitable tool to probe the possible interfacial interaction between carbon nitride and the supported NPs, which can not be easily detected in the literatures. The chemical state of $Ni_{0.5}Co_{0.5}O$-NCN after the reaction is also probed by XAS in Fig. S9.† Both Co and Ni are partly reduced after the hydrolysis reaction (decreased feature A and increased feature B) but still keep some oxidized contents. In the preparation process the reduction solution was slowly dropped in the mixture, then the NPs were deposited on NCN and might be only slightly reduced (mainly oxidized). The exposure to air of NPs might also lead to the oxidized states. Thus the prepared NPs are oxidized. However, the hydrolysis reaction is a fast process with all AB solution quickly injected into the flask, then the NPs on NCN can be partly reduced with large amounts of H_2 and are not easy to be fully oxidized by the exposure to air. The hydrolysis process is also a further reduction when compared to the initial synthesis process, which is easier for the reduction of NPs. Then the NPs after reaction can be partly reduced. The partial reduction of $Ni_{0.5}Co_{0.5}O$ could be the reason for the decreased TOF efficiency as shown in Fig. 2. Metal oxides could be the active reaction sites in the hydrolysis, which show a strong interfacial interaction with NCN to enhance the performance. However, the produced hydrogen will partly reduce the metal oxides and then lower the performance with the formation of less active metal compositions. The TEM images of $Ni_{0.5}Co_{0.5}O$-NCN after the first cycle and the 6th cycle are also shown in Fig. S10,† in which the aggregation of NPs can be observed with the formation of metals.

The working mechanism of $Ni_{0.5}Co_{0.5}O$-NCN can thus be illustrated in Fig. 5. Ni and Co form oxidized NPs of $Ni_{0.5}Co_{0.5}O$ on the substrate of NCN, which has a typical carbon nitride structure. The C and N sites in NCN can act as two different bonding sites to anchor the metal elements with a suitable interfacial interaction, in which C is the electron acceptor while N is the electron donor. Thus a stable interfacial interaction in $Ni_{0.5}Co_{0.5}O$-NCN can form and then accelerate the hydrolysis of AB. The synergistic effect of two metal elements of Ni and Co in the NPs can also facilitate the reaction. Moreover, Ni and Co have similar but different electronegativities, which may also help to form the stable interfacial interaction. The two reaction center structure in carbon nitride may also shed light on the mechanism study of various applications using carbon nitride as the substrate.

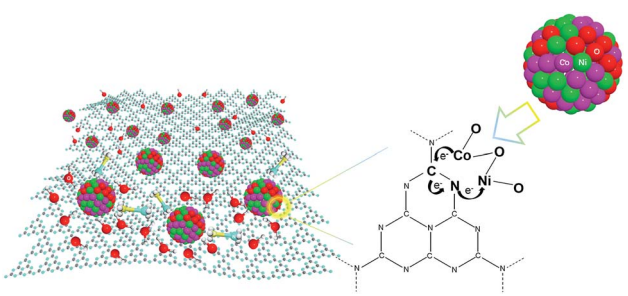

Fig. 5 Illustration of the AB hydrolysis on $Ni_{0.5}Co_{0.5}O$-NCN.

Conclusions

In this work we report a $Ni_{0.5}Co_{0.5}O$-NCN nanostructure for the hydrolysis of AB. The hybrid material shows an excellent TOF value of 76.1 (H_2) mol per (Cat-metal) mol min with a good stability. X-ray absorption spectroscopy reveals that the carbon nitride substrate exhibits a strong interfacial interaction with the NPs, in which C may act as the electron acceptor while N may act as the electron donor. A stable interfacial interaction in $Ni_{0.5}Co_{0.5}O$-NCN can thus form and then accelerate the hydrolysis of AB. The synergistic effect of two metal elements of Ni and Co in the NPs can also facilitate the reaction. The two reaction center structure in carbon nitride may also shed light

on the mechanism study of various applications using carbon nitride as the substrate.

Conflicts of interest

There are no conflicts to declare.

Acknowledgements

We thank SSRF, TLS and NSRL for the support of XAS experiments. We acknowledge the National Natural Science Foundation of China (U1732110). This is also a project supported by Collaborative Innovation Center of Suzhou Nano Science and Technology, Soochow University-Western University Centre for Synchrotron Radiation Research, the Priority Academic Program Development of Jiangsu Higher Education Institutions (PAPD) and the Fund for Innovative Research Teams of Jiangsu Higher Education Institutions.

Notes and references

1 Q. Zhu, J. Li and Q. Xu, *J. Am. Chem. Soc.*, 2013, **135**, 10210–10213.
2 M. Zahmakiran and S. Özkar, *Top. Catal.*, 2013, **56**, 1171–1183.
3 Ö. Metin, V. Mazumder, S. Özkar and S. H. Sun, *J. Am. Chem. Soc.*, 2010, **132**, 1468–1469.
4 H. L. Jiang and Q. Xu, *Catal. Today*, 2011, **170**, 56–63.
5 S. K. Singh, A. K. Singh, K. Aranishi and Q. Xu, *J. Am. Chem. Soc.*, 2011, **133**, 19638–19641.
6 Q. L. Yao, Z. H. Lu, Y. W. Yang, Y. Z. Chen, X. S. Chen and H. L. Jiang, *Nano Res.*, 2018, **11**, 4412–4422.
7 P. Z. Li, A. Aijaz and Q. Xu, *Angew. Chem., Int. Ed.*, 2012, **51**, 6753–6756.
8 C. Y. Peng, L. Kang, S. Cao, Y. Chen, Z. S. Lin and W. F. Fu, *Angew. Chem., Int. Ed.*, 2015, **54**, 15725–15729.
9 Z. Li, T. He, D. Matsumura, S. Miao, A. Wu, L. Liu, G. Wu and P. Chen, *ACS Catal.*, 2017, **7**, 6762–6769.
10 K. Mori, K. Miyawaki and H. Yamashita, *ACS Catal.*, 2016, **6**, 3128–3135.
11 X. H. Zhou, Z. X. Chen, D. H. Yan and H. B. Lu, *J. Mater. Chem.*, 2012, **22**, 13506–13516.
12 M. Chandra and Q. Xu, *J. Power Sources*, 2006, **156**, 190–194.
13 T. B. Marder, *Angew. Chem., Int. Ed.*, 2007, **46**, 8116–8118.
14 Z. H. Lu, J. Li, A. Zhu, Q. Yao, W. Huang, R. Zhou, R. Zhou and X. S. Chen, *Int. J. Hydrogen Energy*, 2013, **38**, 5330–5337.
15 C. C. Hou, Q. Li, C. J. Wang, C. Y. Peng, Q. Q. Chen, H. F. Ye, W. F. Fu, C. M. Che, N. López and Y. Chen, *Energy Environ. Sci.*, 2017, **10**, 1770–1776.
16 Z. C. Fu, Y. Xu, S. L. Chan, W. W. Wang, F. Li, F. Liang, Y. Chen, Z. S. Lin, W. F. Fu and C. M. Che, *Chem. Commun.*, 2017, **53**, 705–708.
17 C. Wang, J. Tuninetti, Z. Wang, C. Zhang, R. Ciganda, L. Salmon, S. Moya, J. Ruiz and D. Astruc, *J. Am. Chem. Soc.*, 2017, **139**, 11610–11615.
18 Q. Yao, K. Yang, X. Hong, X. S. Chen and Z. H. Lu, *Catal. Sci. Technol.*, 2018, **8**, 870–877.
19 K. Feng, J. Zhong, B. Zhao, H. Zhang, L. Xu, X. H. Sun and S. T. Lee, *Angew. Chem., Int. Ed.*, 2016, **55**, 11950–11954.
20 H. Zheng, K. Feng, Y. Shang, Z. Kang, X. Sun and J. Zhong, *Inorg. Chem. Front.*, 2018, **5**, 1180–1187.
21 M. A. Khalily, H. Eren, S. Akbayrak, H. H. Susapto, N. Biyikli, S. Özkar and M. O. Guler, *Angew. Chem., Int. Ed.*, 2016, **55**, 12257–12261.
22 L. Yang, N. Cao, C. Du, H. M. Dai, K. Hu, W. Luo and G. Z. Cheng, *Mater. Lett.*, 2014, **115**, 113–116.
23 X. C. Wang, K. Maeda, A. Thomas, K. Takanabe, G. Xin, J. M. Carlsson, K. Domen and M. Antonietti, *Nat. Mater.*, 2009, **8**, 76–80.
24 P. Niu, L. L. Zhang, G. Liu and H. M. Cheng, *Adv. Funct. Mater.*, 2012, **22**, 4763–4770.
25 W. Wang, Z. H. Lu, Y. Luo, A. H. Zou, Q. L. Yao and X. S. Chen, *ChemCatChem*, 2018, **10**, 1620–1626.
26 L. T. Guo, Y. Y. Cai, J. M. Ge, Y. N. Zhang, L. H. Gong, X. H. Li, K. X. Wang, Q. Z. Ren, J. Su and J. S. Chen, *ACS Catal.*, 2015, **5**, 388–392.
27 H. Zhang, X. J. Gu, P. L. Liu, J. Song, J. Cheng and H. Q. Su, *J. Mater. Chem. A*, 2017, **5**, 2288–2296.
28 P. Liu, X. Gu, K. Kang, H. Zhang, J. Cheng and H. Su, *ACS Appl. Mater. Interfaces*, 2017, **9**, 10759–10767.
29 H. Wang, Y. G. Wang, Y. Zhang, Q. Wang, X. Ren, D. Wu and Q. Wei, *Sci. Rep.*, 2016, **6**, 27385.
30 H. Kahri, M. Sevim and Ö. Metin, *Nano Res.*, 2017, **10**, 1627–1640.
31 M. Groenewolt and M. Antonietti, *Adv. Mater.*, 2005, **17**, 1789–1792.
32 J. Hu, Z. Chen, M. Li, X. Zhou and H. Lu, *ACS Appl. Mater. Interfaces*, 2014, **6**, 13191–13200.
33 D. Marton, K. J. Boyd, A. H. Al-Bayati, S. S. Todorov and J. W. Rabalais, *Phys. Rev. Lett.*, 1994, **73**, 118.
34 J. S. Zhang, M. W. Zhang, L. H. Lin and X. C. Wang, *Angew. Chem.*, 2015, **127**, 6395–6399.
35 B. R. Wulan, S. S. Yi, S. J. Li, Y. X. Duan, J. M. Yan and Q. Jiang, *Appl. Catal., B*, 2018, **231**, 43–50.
36 Y. Zheng, Y. Jiao, Y. H. Zhu, L. H. Li, Y. Han, Y. Chen, A. J. Du, M. Jaroniec and S. Z. Qiao, *Nat. Commun.*, 2014, **5**, 3783.
37 J. Zhong, J. J. Deng, B. H. Mao, T. Xie, X. H. Sun, Z. G. Mou, C. H. Hong, P. Yang and S. D. Wang, *Carbon*, 2012, **50**, 335–338.
38 J. H. Lee, J. Ryu, J. Y. Kim, S. W. Nam, J. H. Han, T. H. Lim, S. Gautam, K. H. Chae and C. W. Yoon, *J. Mater. Chem. A*, 2014, **2**, 9490–9495.
39 J. Zhong, H. Zhang, X. Sun and S. T. Lee, *Adv. Mater.*, 2014, **26**, 7786–7806.